
Check for updates

of B
pendent Bragg
associated with the prev
identified by our GINSES measureme
an established method, there are neutron scattering
are excellently suited for that kind of experiment, whereas for
GINSES measurements the main focus of the instrument construction was in transmission mode. That experimental advantage promised a more speedy experiment than performed otherwise.

This also opened a possibility to further explore the previously assumed temperature behavior of the modes, about which we only hyposized before. By varying the temperature below the liquid disordered phase transition of the membranes (Mortensen et al., 1988; Bultmann et al., 1991) a significant change in the behavior of the mode was expected. Indeed, the correlating structures change, both in abundance as well as in size, with temperature.

The data presented here thus addresses two aspects simultaneously: First, an additional, different method indeed confirms the modes are not an instrumental artefact as GISANS and GINSES are both based on different measurement principles, aiming at structure and dynamics respectively. Second, using the increased speed of measurement a larger temperature interval could be covered, proving the temperature dependent behavior of the modes, which also prove they couple well to the phase behavior of the membrane system, as expected.

That being said, the information that can be retrieved from GISANS measurements about the surface modes of the membranes is limited and only reveals the possible existence of said mode indirectly via the characteristic length scale. There are only very few directly accessible parameters, using only GISANS. Despite that, we still deem the method presented here to be a valuable tool, as it makes scanning a wide range of parameters, such as temperature or concentration, feasible. Finally, also the theoretical aspect of those coherent excitations can be further elucidated by the theoretical calculations based on smectic membrane theory and synthetic created data.

2. Materials and methods

The experimental results in this manuscript have been obtained by GISANS. The data evaluation as well as the computational results are based on software written by the authors (Monkenbusch et al., 2019). The sample preparation followed the protocol as outlined in Jaksch et al. (2015, 2017).

achieve a hy
assembled layer structure the SoyPC (
Polar Lipids) was dissolved in isopropanol p.A. and gently shaken ($\sim$1–2 s^{-1}) until a completely homogeneous solution was obtained (approximately 10 min). Shaking was subsequently continued for another 10 min. The Si-block meanwhile was placed in a frame to prevent the solution from flowing-off of the surface. Subsequently the solution was deposited on the Si-block, which was placed in a vacuum oven and aligned to be horizontal. In order to achieve slow and even drying the oven was left at room temperature, while the inside pressure was regulated to 25 kPa under reflux conditions. This is above the vapor pressure for the solution, thus no bubbling occurred.

After 12 h the maximum vacuum (below 25 kPa) was used to finally dry the sample. Olfactory inspection did not reveal any traces of remaining isopropanol. The Si-block with the deposited sample was then placed into a water tight frame, which was fully filled with D_2O to achieve maximum hydration of the sample. Being placed at the instrument KWS-1 (Feoktystov et al., 2015) the sample was temperature controlled by a water thermostat.

2.2. Instrument setup

2.2.1. GISANS

The GISANS experiments were performed at the KWS-1 (Feoktystov et al., 2015) instrument at the Heinz Mainer-Leibnitz Centre (MLZ), Garching, Germany. As previous attempts were limited by a weak signal to noise ratio and needed to be improved in terms of optimized instrument resolution, pixel size and background (Jaksch et al., 2018) a pinhole setup was chosen, where the size of the sample aperture is ideally mapped to the size of a pixel on the detector. This was achieved by using a 7 × 7 mm, a collimation length of 20 m and a sample-detector distance of 14 m. As the pixel size is 8 mm in both directions, this leads to a near optimal mapping on the detector and very low background.

The incident angle in all cases was 0.2°.

2.3. Data evaluation

The data was normalized using the qtiKWS software as provided

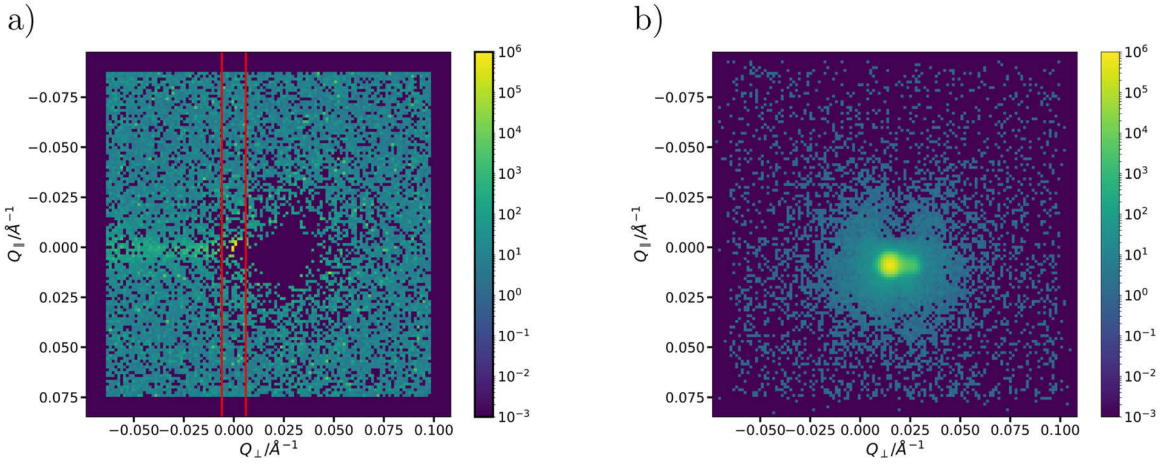

Fig. 1. (a) Representative scattering image at initial conditions and 37 °C, the red lines indicate the area of averaging for the in-plane cut. (b) Image of direct beam with beamstop removed.

(Pip
written by th
Fortran script describe
(Monkenbusch et al., 2019).

A representative detector image can be seen in
beam had to be shadowed to achieve a good signal to noise ratio, he
the low signal area in the center of the image. The final in plane cut is the averaging over both sides (top and bottom) of the in-plane cut shown. There was no averaging in $Q_{\parallel}$-direction. Since the sample aperture was ideally matched to the pixel size, a sharp peak would also present as a single pixel with higher intensity than its surroundings.

3. Results

In order to illuminate both the experimental data as well as the theory used for the interpretation of that data, this section is separated into GISANS results and computational results, where calculations based on the paper by Romanov and Ul'yanov (2002) for supported smectic membranes are presented.

3.1. GISANS

Beginning at 37 °C the sample was cooled down in several steps to 16 °C and then reheated to inital conditions. The sample was equilibrated for 15 min before each measurement. Where appropriate, earlier results of GINSES measurements are correlated with the GISANS results. An overview over the results is given in Fig. 2. The clear position of the first dynamic peak shows the characteristic length of the detected mode. There are several areas in the temperature map that shall be discussed here. The first and most striking feature is that the position of one main peak at values slightly below $Q_{\parallel} = 0.01$ Å^{-1} and one or two higher order peaks can be distinguished at any temperature, except for the coexistence area of the L_{α} and L_{β} phase. Even though the statistical significance in the case of a single scattering curve is low, since the maximum is only one point due to the detector resolution, considering all curves together as done in Fig. 2(a) shows the presence of those peaks. The coexistence area then is also the area where a hysteresis of the extracted correlation length parameter $\lambda_{\text{phase}} = 2\pi/Q_{\parallel}^{\text{max}}$ (see Fig. 4), can be observed. This hysteresis is true for most of the parameters discussed here. Another striking feature is that seemingly the peak position is extremely stable against temperature variation within one phase. Looking at the extracted characteristic length λ_{phase} in Fig. 4(a) this is however revealed to be not strictly true in all cases and to be a visual misconception in some cases, when the peaks are extremely broad or ill defined by being simply a single point. For a better understanding of this one should consider the sample history. The heating ramp
fitting algorithm finds a higher χ^2 when
does not reflect a real uncertainty.

Apart from the correlation length the overall intensity of the excitations is of interest. Here the amplitude of the Gaussian fits shown in Fig. 2(b) is directly proportional to the abundance of excitations per unit area in the membrane. The corresponding data is shown in Fig. 4. The amplitude of the first peak consistently drops from 27 to 10 cooling down to 31 °C, interestingly without an apparent phase transition and again drops below the L-β phase transition down to 5. Upon reheating nearly the full amplitude is recovered and the amplitude is developing with increasing temperature in a comparable manner as when being cooled down. The consistent drop is interrupted by the data point at $T = 31$ °C. The fitting for that specific point however was very unstable and we therefore do not include this deviation in our analysis.

From these data we can conclude that the density of excitations is higher above $T = 25$ °C and decreases by a factor of five between 37 and 16 °C. So, apart from the phase transition around 22 °C the consistently highest density of excitations occurs around physiological temperatures. This density of excitations can generally be associated with the energy density in the membrane, while the width of the peak is a measure of the different contributing wavelengths to that specific excitation, i.e. the wavelength distribution. While the steep increase towards body temperature is only signified by a single point, the value is also nearly regained after heating.

3.2. Computational

At first, it should be noted that we do not present simulated data here, in the sense that some kind of Monte Carlo simulation is presented, but rather an execution of the equations by Romanov and Ul'yanov (2002) with appropriate values and boundary conditions, the computations were performed with the parameters given in Table 1. The corresponding code is discussed in our publication about the used software (Monkenbusch et al., 2019).

In order to extract the dynamic contribution from code that essentially only produces the intermediate scattering function as in NSE the intermediate scattering functions were fitted with the expression $S(Q, \tau)/S(Q, \tau = 0) = (1 - A)\exp((G_1\tau)^{\beta}) + A\exp(-G_2\tau)\cdot\cos(\omega\tau) + \text{const}$. Here A is the amplitude of the oscillation, G_1 and G_2 are the decay

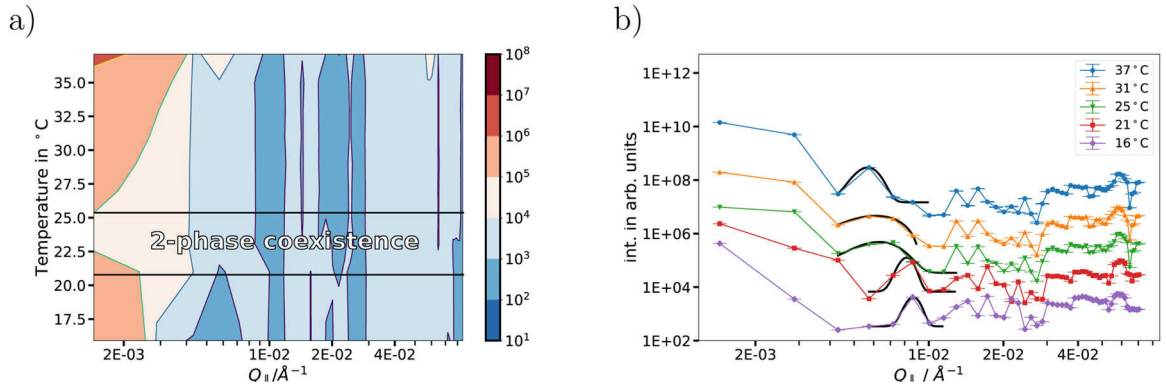

Fig. 2. (a) Temperature vs. intensity map for all recorded scattering data during the cooling phase. There are several regions that can clearly be identified, such as the peak regions and the coexistence region for the L-α and L-β phase. (b) Representative intensity vs. scattering vector $Q_{\parallel}$ plots as were used to create (a). The curves are shifted by factors of 10^1 to 10^4 (bottom to top) for better visibility. The fits (black lines) show both the resulting curves as well as the fitting interval that was used to create them.

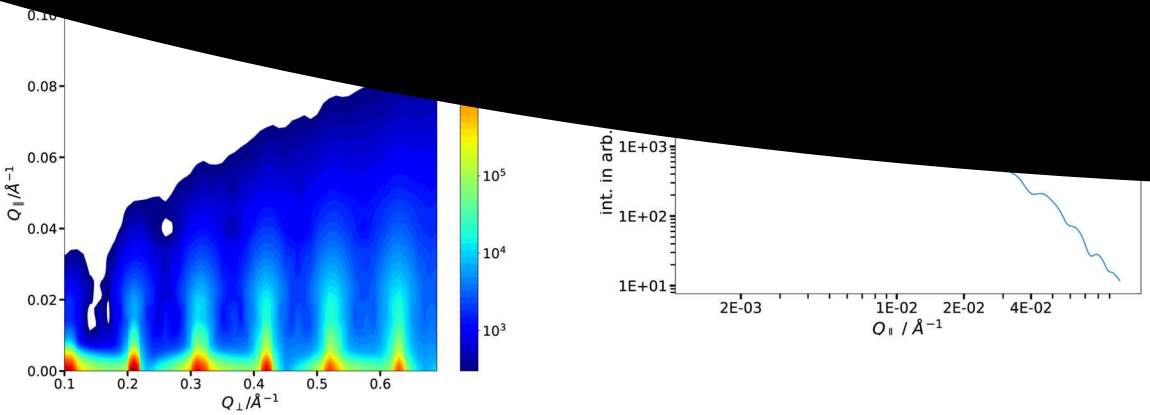

Fig. 3. (a) Calculated GISANS image with the parameters as shown in Table 1. The out-of-plane cut clearly shows the lamellar spacing of the phospholipid membranes, while the in-plane structure is only visible in the low intensity regions between the out-of-plane peaks. (b) In-plane cut at $Q_\perp = 0.18$ Å^{-1} similar to the data obtained in Fig. 2(b).

constants for the purely elastic and the coherent excitation contribution, respectively, β is the stretching parameter and ω the frequency of the oscillation. A constant for the plateau at long Fourier times is added. Here the amplitude A can be associated with the presence of a dynamic contribution, without it a simple exponential decay is observed.

Representative corresponding fits are shown in Fig. 5(a).

The resulting amplitude for a range of Q-values is then used to gauge the contribution of the coherent excitation, which results in a plot that reproduces the location of the peaks in the cuts of the measured GISANS images very well. Here it is important to note, that the data in Fig. 5(b) is not connected to the intensity distribution as observed in GISANS, but merely shows the abundance of the previously mentioned modes on the length scale associated with the respective $Q_\parallel$-values.

When compared with the previously published measured GINSES data, the correct location of the minima and maxima of the intermediate scattering function cannot be replicated. However, the qualitative behavior and the Q-dependency are identical. Indeed, the extracted structural features from GISANS coincide with the maxima calculated for the amplitudes in the intermediate scattering function. Also, the maxima and minima of the calculated in-plane cut show shifted maxima in intensity when compared to the measured GISANS data. We attribute this to the fact that the theory is expecting infinitely thin layers, while the real bilayers have a physical thickness.

We also used the algorithms to create a GISANS image directly only from the deduced data. The resulting image is shown in Fig. 3(a). The structures as investigated in the GISANS data above can also be seen here in the areas of lower intensity between the out-of-plane peaks of the lamellar structure. This also explains, that the simple assumption of having flexible membranes with undulations can lead to the observed data. This is further illustrated by an in-plane cut shown in Fig. 3(b). The structures, albeit at slightly shifted $Q_\parallel$-values are visible, and as there is no incoherent background in the simulation, also more higher order peaks can be seen.

Table 1
Input parameters for calculated scattering curves as shown in Fig. 5. Other parameters were kept constant at 10 total layers, $d = 6$ nm repeat distance and $\rho = 1000\,\mathrm{kg\,m^{-3}}$ density.

	35 °C
Compression modulus B/Pa	3.0×10^6
Surface tension γ/N m	0.03
Intra-membrane viscosity η_3/Pa s	7.5×10^{-3}
Bending modulus κ/k_BT	19

4. Discussion and conclusions

Combining the results shown above with our previous results on the dynamics of phospholipid membranes (Jaksch et al., 2017) a new image emerges. We now can clearly separate the out-of-plane structure of the membranes on a length scale of ≈6 nm and an in-plane correlation which we can link to the dynamics observed in GINSES of ≈100 nm. The measurements presented here also allow to observe a temperature

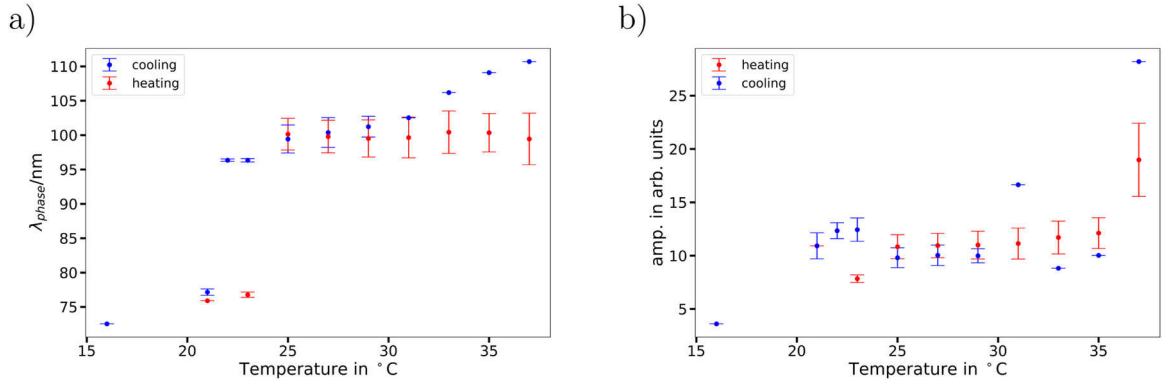

Fig. 4. (a) λ_{phase} wavelength for the in-plane correlations described by the peaks found in the in-plane cuts of the GISANS data. (b) Amplitudes for all peaks at all temperatures from data in Fig. 2.

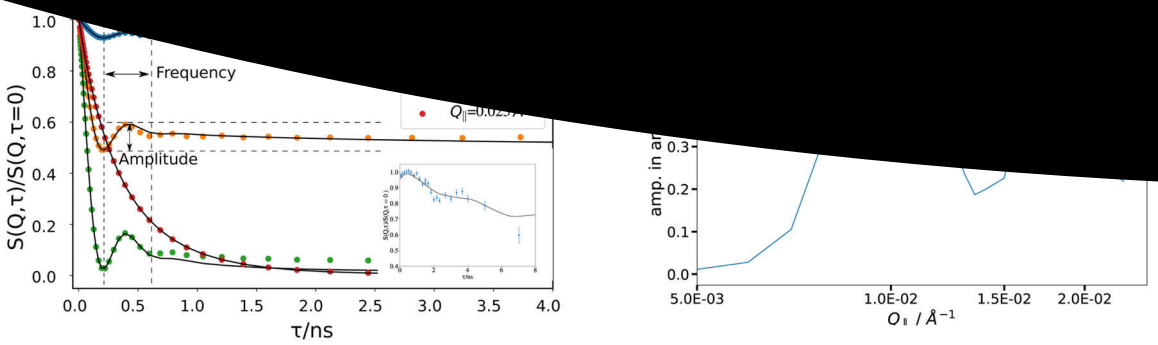

Fig. 5. (a) Overview of fits of the computed intermediate scattering function for representative Q-values. While the frequency remains constant the amplitude of the coherent contribution is strongly Q-dependant. The inset shows the measured GINSES data from our previous publication (Jaksch et al., 2017). While we were not able to reproduce completely identical figures by computation, the qualitative similarity is striking. (b) Amplitudes of the fits shown in (a).

dependence of the in-plane structures. This leads to the conclusion that the features we are describing here are indeed associated with the membrane modes as shown above and therefore of a dynamic nature. The variables and parameters used for computation in this section are described in Table 1. They are based on the data presented in this manuscript and our previous manuscript (Jaksch et al., 2017).

One question that is left open is the exact nature of the excitations in real space. There are a range of possible modes for a collective motion of a membrane stack, such as undulations, peristaltic modes, baroclinic modes and second sound modes (Gelbart et al., 2012). Here it is worth mentioning that those modes who are originally considered to be present in single bilayer systems are on the length-scale of the thickness of that bilayer, while here longer distances are probed. A few considerations can however be made. Since the observations are strictly in plane, and no out-of-plane contribution is visible, we can assume a strict in-plane density correlation. Also, the lower modes as described by the Romanov calculations (Romanov and Ul'yanov, 2002) would necessarily move the complete layer stack, which seems unlikely. The last consideration concerns the peristaltic mode. In this case, as it would be between the bilayers, a transport of water is to be expected, which introduces additional friction and energy constraints to that mode, which at least seem unlikely. So, in the absence of experimental evidence one way or the other, undulations or density fluctuations as in an acoustic wave seem to be the most likely options.

Taken altogether, the measurements show the following picture: (1) There are excitations in phospholipid membranes, (2) these excitations are associated to sufficiently regular structures to be observed in a time and spatially averaging method such as GISANS and (3) the involved energies are below the threshold to be thermally excited (on the order of $h\nu \approx 1\,\mu\text{eV}$ for a single excitation from GISANS and GINSES).

Considering the length scales and energies involved in those systems we can speculate on the effects by the excitations discussed above. The modes as such have energy, lifetime and speed. Taking those properties together they can be considered fundamental for properties such as energy transport along a membrane, and also for dissipation of that energy over a certain area. Energies that are thermally available in such systems usually amount to $\sim k_B T$, which is consistent with the activation energies found in GINSES. Larger energies then can be dissipated or transported in membrane patches, which can contain multiple excitations at a time. Also, the width of the peaks in GISANS hints to the fact that a range of single excitations with subtly different frequencies contribute to the overall undulation, otherwise sharper peaks would be expected. Each of the single excitations however has an energy low enough to be easily excited at room temperature. This could help to dissipate local high energy densities to prevent membrane damage. Also, as they are an in-plane correlation this modes could play a role in the transport of larger objects, such as membrane proteins that otherwise might be sterically or enthalpically suppressed, analogous to flotsam being transported by a wave.

A comparison with biologic systems the energies and length scales associated with E. Coli bacteria can be considered (Swiecicki et al., 2013). The overall length of a bacterium is on the order of 2–4 μm and the cross section diameter is $\sim 1.5\,\mu\text{m}$. Diffusion speeds along the membrane are on the order of a few $\mu\text{m}\,\text{s}^{-1}$. Thus we know that an excitation as reported here can travel along the bacterium as the propagation range is virtually identical to the dimensions of the bacterium (calculated from a 2 ns frequency and lifetime of the same order from GINSES and the speed of sound of $1500\,\text{m}\,\text{s}^{-1}$ in water). Additionally, considering the speed and dimensions, the kinetic energy during diffusion of a bacterium is on the order of $\sim 5\,\mu\text{eV}$, which coincides with the energy of a single mode of the coherent excitations with $\hbar\omega = \hbar\,{}^{2\pi}/_{2\text{ns}} \approx 5\,\mu\text{eV}$. Another striking fact is, that the abundance of excitations seems to have a maximum at physiological temperatures, which at least suggests a biological relevance.

Thus, energy from external stimuli or temperature which can be expected to occur in such a system can be transported with ease along the membrane. This transport and dissipation of energy can potentially help prevent a rupturing of the membrane and contribute to its biological function.

From a fundamental physics point of view, these excitations exhibit all properties expected from quasi-particles such as phonons. Since they however depend on a lamellar structure of the system they are distinct from them, which makes them *surface mode phonons* or *smomons*.

Conflict of interest

All authors are employees of the Forschungszentrum Jülich GmbH. The work published here did not receive external funding or grants.

The authors declare no conflict of interest, financial or otherwise.

Acknowledgements

We gratefully acknowledge the granting of beamtime by both the Heinz Maier-Leibnitz Zentrum, Garching, Germany, as well as the Spallation Neutron Source, Oak Ridge/TN, USA.

Furthermore we thank Dr. Michael Monkenbusch for the development of the Romanov calculation code and the support in performing the calculations.

References

Armstrong, C.L., Toppozini, L., Dies, H., Faraone, A., Nagao, M., Rheinstädter, M.C., 2013. Incoherent neutron spin-echo spectroscopy as an option to study long-range lipid diffusion. ISRN Biophysics 2013.

Armstrong, C.L., Häußler, W., Seydel, T., Katsaras, J., Rheinstädter, M.C., 2014.

(15), 260…
Bultmann, T., Lin, H.N., …
havior of mixed-chain phospha…
l-.alpha.-dipalmitoylphosphatidylcholine. Bi…
Caille, A., 1972. Remarques sur la diffusion des rayons x dan…
Sci. Ser. B 274, 891–893.
Cevc, G., 1997. Drug delivery across the skin. Expert Opin. Investig. Drugs 6 (12), 1887–1937.
Constantin, D., Brotons, G., Salditt, T., Freyssingeas, É., Madsen, A., 2006. Dynamics of bulk fluctuations in a lamellar phase studied by coherent X-ray scattering. Phys. Rev. E 74 (3), 031706.
Feoktystov, A.V., Frielinghaus, H., Di, Z., Jaksch, S., Pipich, V., Appavou, M.-S., Babcock, E., Hanslik, R., Engels, R., Kemmerling, G., et al., 2015. Kws-1 high-resolution small-angle neutron scattering instrument at JCNS: current state. J. Appl. Crystallogr. 48 (1), 61–70.
Fragneto, G., Rheinstädter, M., 2007. Structural and dynamical studies from bio-mimetic systems: an overview. Comp. Rend. Phys. 8 (7–8), 865–883.
Gelbart, W.M., Ben-Shaul, A., Roux, D., 2012. Micelles, Membranes, Microemulsions, and Monolayers. Springer Science & Business Media.
Jaksch, S., Lipfert, F., Koutsioubas, A., Mattauch, S., Holderer, O., Ivanova, O., Frielinghaus, H., Hertrich, S., Fischer, S.F., Nickel, B., 2015. Influence of ibuprofen on phospholipid membranes. Phys. Rev. E 91 (2), 022716.
Jaksch, S., Schulz, A., Di, Z., Luxenhofer, R., Jordan, R., Papadakis, C.M., 2016. Amphiphilic triblock copolymers from poly(2-oxazoline) with different hydrophobic blocks: changes of the micellar structures upon addition of a strongly hydrophobic cancer drug. Macromol. Chem. Phys. 217 (13), 1448–1456.
Jaksch, S., Holderer, O., Gvaramia, M., Ohl, M., Monkenbusch, M., Frielinghaus, H., 2017. Nanoscale rheology at solid-complex fluid interfaces. Sci. Rep. 7 (1), 4417.
Jaksch, S., Koutsioubas, A., Mattauch, S., Holderer, O., Frielinghaus, H., 2018. Preliminary Report on Measurements of Dynamic Contributions to Coherent Neutron Scattering. . arXiv:1803.11041.
Mortensen, K., Pedi…
phosphatidylcholine-cholesterol system a…
ripple structure and phase diagram. Biochim. Biophys. Acta (BBA) – Biomembranes 945 (2), 221–245.
Pipich, V., 2012. QtiKWS: User-Friendly Program for Reduction, Visualization, Analysis and Fit of SA(N)S Data.
Romanov, V.P., Ul'yanov, S.V., 2002. Dynamic and correlation properties of solid supported smectic-a films. Phys. Rev. E 66 (6), 9 ISI Document Delivery No.: 635YD Times Cited: 19 Cited Reference Count: 27 Romanov, VP Ul'yanov, SV Romanov, Vadim/J-6874-2013 19 AMER PHYSICAL SO, COLLEGE PK PHYS REV E 1.
Salditt, T., 2005. Thermal fluctuations and stability of solid-supported lipid membranes. J. Phys.: Condens. Matter 17 (6), R287.
Swiecicki, J.-M., Sliusarenko, O., Weibel, D.B., 2013. From swimming to swarming: *Escherichia coli* cell motility in two-dimensions. Integr. Biol. 5 (12), 1490–1494.
Tanaka, M., 2013. Physics of interactions at biological and biomaterial interfaces. Curr. Opin. Coll. Interface Sci. 18 (5), 432–439.
Touitou, E., Dayan, N., Bergelson, L., Godin, B., Eliaz, M., 2000. Ethosomes-novel vesicular carriers for enhanced delivery: characterization and skin penetration properties. J. Control. Release 65 (3), 403–418.
Wolkers, W.F., Looper, S.A., Fontanilla, R.A., Tsvetkova, N.M., Tablin, F., Crowe, J.H., 2003. Temperature dependence of fluid phase endocytosis coincides with membrane properties of pig platelets. Biochim. Biophys. Acta (BBA) – Biomembranes 1612 (2), 154–163.